Oxygen effects on ω and α phase transformations in a metastable β Ti-Nb alloy

Kathleen Chou, Emmanuelle A. Marquis*

Department of Materials Science and Engineering, University of Michigan, Ann Arbor, MI 48109 USA;

**Corresponding Author*

Kathleen Chou
Dow Building
2300 Hayward St.
Ann Arbor, MI 48109
kachou@umich.edu
Phone: 248-925-7880
ORCID: 0000-0003-1974-4766

Emmanuelle A. Marquis (Corresponding Author)
Dow Building
2300 Hayward St.
Ann Arbor, MI 48109
emarq@umich.edu
Phone: 734-764-8717
ORCID: 0000-0002-6476-2835

Oxygen effects on ω and α phase transformations in a metastable β Ti-Nb alloy

Kathleen Chou[a], Emmanuelle A. Marquis[a*]

[a] *Department of Materials Science and Engineering, University of Michigan, Ann Arbor, MI 48109 USA*

**Corresponding Author*

Graphical Abstract

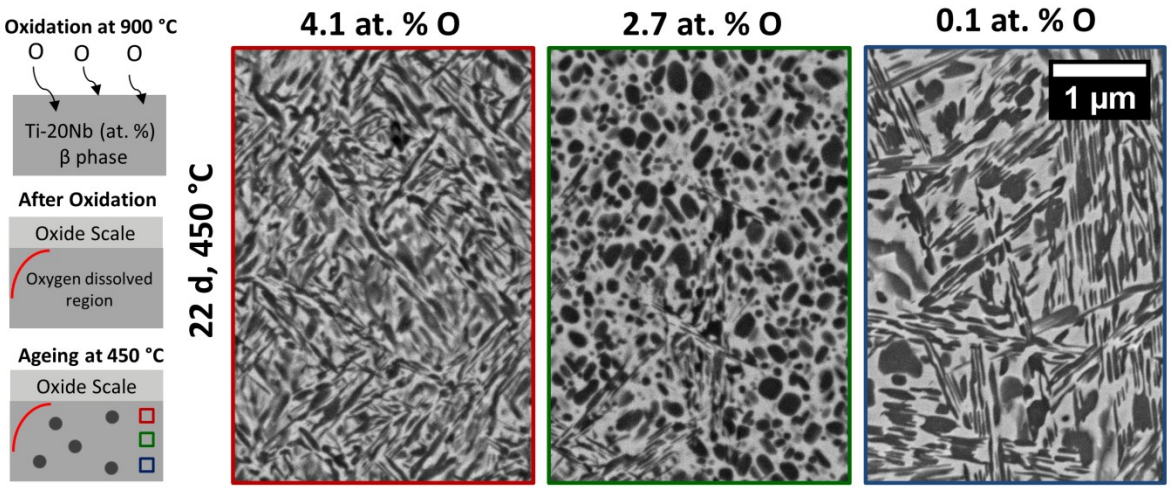

Abstract

Oxygen is known to have substantial influence on metastable β titanium alloys through martensite suppression and phase stability changes that significantly affect mechanical behavior. Here, we have investigated the influence of oxygen in solid solution on ω and α precipitation during ageing in a metastable β-type Ti-20Nb atomic (at.) % alloy with up to about 5 at. % O obtained through an oxidation exposure. Ageing results show that elevated oxygen induced a shape change for ω precipitates from an ellipsoid shape to an elongated rod shape and resulted in a higher ω number density. Additionally, the growth rate of ω precipitates was slowed with oxygen. Oxygen partitioned to the ω phase during ageing and was shown to expand the region of ω phase stability to higher temperatures, suggesting that oxygen increases ω phase stability. Prolonged ageing revealed that α eventually nucleated at all oxygen levels. However, the rate of α precipitation depended on oxygen content, and the slowest rate was observed with intermediate levels of oxygen (~2-3 at. %) compared to elevated and minimal levels. A mechanism for this

non-linear effect on α precipitation is discussed based on oxygen acting as both an ω-stabilizer and α-stabilizer in β titanium alloys.

Keywords

Titanium alloys, Phase transformations, Precipitation, Omega phase, Oxygen

1. Introduction

Phase stability in the metastable β titanium alloy system has been an active area of investigation to develop alloys intended for applications including aerospace and biomedical industries [1]. The bcc β phase matrix that can be stabilized to room temperature with the addition of β-stabilizing elements such as Mo, V, and Nb is particularly sensitive to alloy composition and heat treatment [2]. In addition to precipitation of the stable hcp α phase, minor changes in composition and processing can result in formation of metastable phases including hexagonal ω, martensites α' (hcp) and α" (orthorhombic) [3]. At high concentrations of β phase stabilizers, spinodal decomposition has also been reported [1, 3]. These various instabilities lead to a rich variety of microstructures that have been widely explored in literature [1, 4, 5]. Specific chemistries and heat treatment paths for β Ti alloys are tailored to their anticipated use areas, with aerospace alloys desiring a fine precipitation of α phase for high strength [6] and biomedical alloys requiring sufficient control of metastable phase formation to obtain a low Young's modulus and controlled deformation behavior [7, 8].

Oxygen has been shown to have a significant influence on titanium alloy phase stability and performance. Generally, oxygen has extensive solubility in α and β before forming oxide phases, and O is known as a strong α stabilizing element. Dissolved oxygen in the α and β phases causes hardening from interstitial solid solution strengthening and reduces ductility [9]. Additionally, β Ti alloys that have been developed for biomedical applications primarily utilize Nb to stabilize the β phase due to its biocompatibility [7]. These alloys have shown extraordinary changes in mechanical behavior with the addition of oxygen up to 3 at. % in solid solution. One of the first gum metal alloys developed by Saito et al. required 0.7 to 3.0 at. % O to observe desirable properties such as ultralow modulus and superelastic mechanical behavior [10]. More recent studies have demonstrated that oxygen suppresses the formation of martensitic α" upon solution treatment and induces a nanodomain arrangement [11]. Detailed investigations have

suggested that these nanodomains are composed of lattice modulations due to relaxation of local strain fields around oxygen atoms, but formation of long range martensite is inhibited [11]. Stress-induced martensite and deformation twinning [12] during tensile deformation are also suppressed in the presence of oxygen, leading to a suppression in shape memory behavior and increased superelasticity [13, 14]. The suppression of the stress-induced martensitic transformation resulted in non-linear elastic behavior with high oxygen levels [14]. Oxygen has also been shown to influence thermal expansion properties, with a negative linear expansion coefficient observed at 1.2 at. % O in as-rolled Ti-21Nb [15]. Thus, oxygen has important effects on phase stability in β Ti alloys and can dramatically influence the resulting mechanical behavior.

Conflicting results have been reported for oxygen effects on metastable ω phase stability in β Ti alloys. Oxygen has been known to suppress the formation of the ω phase during solution treatment and quenching [16, 17]. First principles calculations suggested that added oxygen increases the energy barrier for phase transition from β to ω [18]. Oxygen has also been reported to reduce the amount of ω that is formed during ageing [19, 20] and cold working [21]. However, more recent studies suggested that ω phase becomes more thermodynamically stable with additions of oxygen after various ageing treatments, with the ω phase being retained instead of fully transforming to the α phase in alloys containing higher oxygen concentrations [22, 23]. The presence and relative stability of the ω phase is of recent interest for metastable β Ti alloys due to its rising importance in influencing deformation behavior. This includes the role of ω phase as a potential heterogeneous nucleation site for α phase precipitation in aerospace β Ti alloys [24-28] and its influence in changing the deformation behavior from transformation-induced plasticity (TRIP) and/or twinning-induced plasticity (TWIP) mechanisms to dislocation channeling [29, 30]. Deformation-induced ω phase has also been reported in β Ti alloys [31]. Finally, fine distributions of ω phase may enhance yield strength while preserving ductility [32, 33]. Thus, clarifying the phase stability of ω with oxygen in metastable β Ti alloys will result in a more nuanced understanding of precipitation behavior and consequently better control of mechanical properties.

In the present work, the precipitation behavior of a model metastable β-type Ti-20Nb (at. %) alloy was studied to elucidate the effects of oxygen on ω and α phase stability. A model binary alloy was selected in order to understand precipitation without the compounding effects of

additional elements in complex engineering alloys. We utilized the extensive solubility and dissolution of oxygen in titanium alloys during high temperature oxidation exposures to obtain specimens with a wide range of dissolved oxygen contents in the β phase matrix. These compositionally graded specimens allowed the investigation of a range of oxygen levels in solid solution up to 5 at. % O. Subsequent ageing heat treatments on pre-oxidized and unoxidized (with very little oxygen) specimens were conducted at temperatures in the ω + α and α phase field regions to understand the precipitation and phase transformation sequence. The influence of oxygen on ω and α precipitation is discussed based on thermodynamic phase stability, kinetic effects, and changes in nucleation driving force.

2. Experimental Methods

An arc-melted button with a nominal composition of Ti-32.7 wt. % Nb (Ti-20 at. % Nb) was provided by ATI. The button was remelted three times to improve homogeneity. Interstitial oxygen levels were measured in the arc-melted button as 0.019 wt. % (0.1 at. %) by inert gas fusion using a LECO analyzer. Specimens were cut from the button using a slow-speed diamond saw, encapsulated with pure Ti pieces in a quartz tube backfilled with Ar gas, and solution treated at 1000 °C for 10 h, quenching by breaking in water. Interstitial oxygen levels after solution treatment were measured as 0.021 wt. % O (0.1 at. %) by inert gas fusion in a LECO analyzer. A subset of solution treated specimens were placed in an Al_2O_3 crucible and oxidized at 900 °C for 5 h in a 1 standard cubic centimeter per minute (SCCM) O_2/4 SCCM Ar environment (approximately pO_2 = 0.2 atm/20.3 kPa) using a Thermo Scientific Lindberg Blue M tube furnace. The oxidation exposure was such that specimens were inserted in the hot zone of the furnace after it was heated to 900 °C in a flowing Ar (40 SCCM) gas environment. After insertion and temperature equilibration back to 900 °C (approximately 15 minutes), the aforementioned oxidizing environment was introduced. Following the oxidation exposure, oxygen gas flow was stopped. Specimens were removed from the hot zone and cooled to room temperature in flowing Ar (40 SCCM). These specimens were termed as “pre-oxidized”.

As-solution treated specimens and pre-oxidized specimens were subsequently aged at 450 °C for 2 hours and 1, 3, 6, 14, 22, and 31 days. This particular ageing temperature was chosen due to it being near the reported upper limit of ω phase stability and therefore would show the ω to α transformation after prolonged ageing [3]. Finally, a set of as-solution treated specimens and

pre-oxidized specimens underwent a two-step heat treatment: first aged at 450 °C for 3 d, then aged a second time at 600 °C for 1 h in order to promote ω phase dissolution and α precipitation. All ageing heat treatments were conducted with samples encapsulated in quartz tubes with pure Ti pieces that were backfilled with Ar gas and quenched by breaking the tubes in water.

Specimens for characterization using scanning electron microscopy (SEM) imaging were mounted and ground using 320-1200 grit SiC papers followed by polishing with 0.03 μm colloidal silica suspension. Wavelength dispersive spectroscopy (WDS) analyses were conducted on polished cross sections of pre-oxidized Ti-20Nb in order to measure dissolved oxygen content in the matrix. WDS allows for more accurate quantification of light elements such as O compared to energy dispersive spectroscopy. These measurements were performed using a Cameca SX100 electron microprobe and collected using an accelerating voltage of 15 kV, beam current of 20 nA, and a focused beam. Intensity correction was performed using the ZAF (Armstrong/Love Scott) method [34]. Standards for microprobe analysis background subtraction for the Kα or Lα x-ray lines for O, Nb, and Ti were collected using MgO (synthetic), $LiNbO_3$ (synthetic), and Ti metal, respectively, with a 30 s peak and 30 s background counting time. Interference correction to deconvolute overlapping peaks of collected spectra was performed using pure Ti metal as the interference correction standard according to the method described in Ref. [35]. SEM imaging and focused ion beam (FIB) preparation of site-specific transmission electron microscopy (TEM) foils and needle-shaped atom probe tomography (APT) specimens were performed using a Thermo-Fisher Scientific FEI Helios Nanolab 650 with a Ga^+ ion FIB. TEM foils were further thinned using broad Ar ion milling in a Gatan PIPS II instrument. TEM images and selected area electron diffraction (SAED) patterns were obtained using a JEOL 3011 microscope operated at 300 kV. A region for 3D FIB tomography was prepared and imaged using a Thermo Fisher Scientific FEI Helios Nanolab 650. Bulk FIB milling of the tomography site was performed at 30 kV, 21 nA, and cleaning steps were performed at 30 kV, 2.5 nA. Individual slices for FIB tomography were milled using a 3 nm slice thickness at 30 kV, 80 pA. FIB tomography images were reconstructed using Avizo software 9.2.0. APT data collection was performed with a Cameca local electrode atom probe (LEAP) 5000 XR operated in laser mode. APT data was collected using a specimen temperature of 30 K, a detection rate of 0.005 atoms per pulse, laser pulse energy of 25 pJ, and pulse repetition rate of 200 kHz. Data reconstruction,

background subtraction, peak deconvolution, and compositional analysis were performed using the Integrated Visualization and Analysis Software (IVAS) package 3.8.2.

3. Results

3.1 Solution treated and pre-oxidized microstructures

The initial microstructure in the solution treated condition showed large β grains (> 1 mm) with α" martensite that formed upon water quenching to room temperature. Martensite formation is consistent with prior literature showing that the martensite start temperature for 20 at. % Nb is about 200 °C [3]. No athermal ω phase was observed in the as-solution treated samples.

In the pre-oxidized samples, the elevated temperature oxidation exposure resulted in the formation of a 60 μm thick layered oxide scale and long α phase laths in the subsurface metal region of the β matrix (**Fig. 1**). The α lath region extended approximately 120 μm into the subsurface metal region of the cross section. α phase formation is attributed to the dissolution of oxygen in the subsurface region of the Ti matrix during oxidation, which thermodynamically stabilizes α at the oxidation temperature [1]. The oxidation behavior and propagation of the α layer are not the focus of this work and will be published elsewhere. SEM backscatter (SEM-BSE) images of the subsurface metal region reveal a microstructural transition to faint laths at the interface between the α + β region and β phase matrix (**Fig. 2a**). SAED patterns and bright field TEM (BF-TEM) micrographs taken from a TEM sample in the matrix near the (α lath + β) / β matrix interface reveal that the matrix is actually composed of α" martensite (**Fig. 2b**) after the oxidation exposure. WDS measurements conducted on a cross section of a pre-oxidized specimen confirmed the ingress of dissolved oxygen in the alloy below the α lath + β region. Data points and error bars for WDS data in **Fig. 2c** report average values and one standard deviation based on five line traces. Data points collected from line traces in the matrix (**Fig. 2c**) show that oxygen levels exponentially decayed from approximately 5 at. % at the (α lath + β) / β matrix interface closer to the sample edges to approximately 1.5 at. % in the center of the cross section. We note that possible experimental sources of error may also originate from surface oxide contributions systematically raising the apparent oxygen concentration [36]. However, bulk atom probe tomography measurements from the center region also show an oxygen concentration of 1.2 at. %, which is within the error bars of the asymptote for WDS oxygen

concentration measurements. Additionally, the WDS data suggest that greater than 5 at. % O (measured at the (α lath + β) / β matrix interface) is needed in order to sufficiently stabilize α phase formation during oxidation at 900 °C for Ti-20Nb. The measured Nb content in the matrix region using WDS was roughly 19 at. %, which agrees with the nominal button composition.

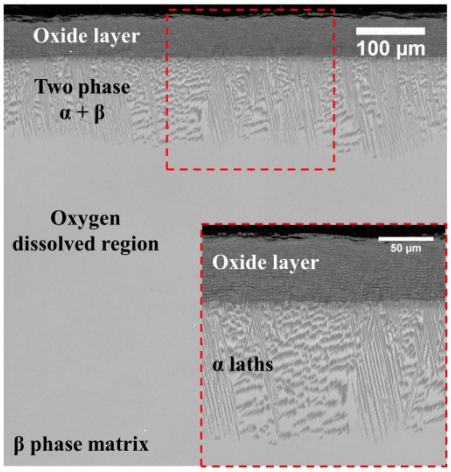

Fig. 1. Cross-sectional SEM-BSE image of Ti-20Nb (at. %) oxidized for 5 h at 900 °C in a 20% O_2/Ar environment. Inset shows higher magnification image of location in red box showing oxide cross section and α lath formation in subsurface metal.

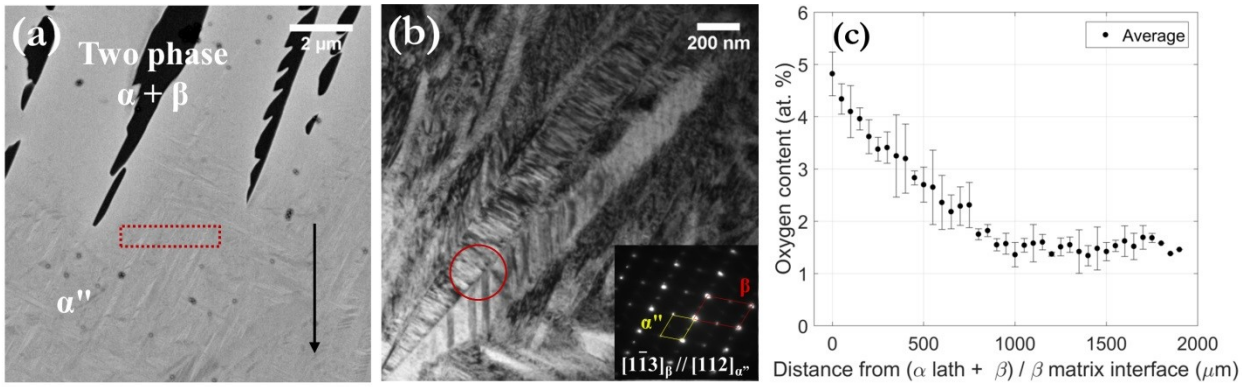

Fig. 2. (a) SEM-BSE cross-sectional image showing microstructural transition at the (α lath + β) / β interface of oxidized Ti-20Nb (at. %). (b) BF-TEM and SAED pattern from location in red circle showing martensite formation of a TEM sample taken from region outlined by red box of oxidized Ti-20Nb. (c) WDS average line traces measuring oxygen content beginning from the (α lath + β) / β interface and traversing across the cross section of oxidized Ti-20Nb (direction of black arrow in Fig. 2a).

3.2 Aged microstructures at 450 °C

As-solution treated samples and pre-oxidized samples were subsequently aged at 450 °C for 2 hours and 1, 3, 6, 14, 22, and 31 days to observe ω and α phase transformations in the β matrix. The as-solution treated and aged samples (with minimal - 0.1 at. % O - and uniform oxygen concentration) are hereafter referred to as *directly aged* (DA) samples, and the pre-oxidized and aged samples (with the created oxygen gradient) are referred to as *oxidized and aged* (OXA). Investigation at different cross-sectional depths from the (α lath + β) / β matrix interface corresponded to microstructures with different oxygen contents, correlating with WDS data presented in **Fig. 2c**, while directly aged specimens were investigated to compare microstructures with 0.1 at. % O. These oxygen levels created during oxidation are assumed to be fixed during ageing due to a slow oxygen diffusion coefficient in β Ti at the ageing temperature [37] and oxygen partitioning behavior to ω and α during annealing [22].

SEM backscatter images (**Fig. 3a-b**) of DA (0.1 at. % O) and OXA (4.8 at. % O) Ti-20Nb specimens after 2 h of ageing at 450 °C reveal dense second phase precipitates at both oxygen levels. These precipitates are identified as ω phase by electron diffraction (**Fig. 3c-d**), with the $[110]_\beta$ SAED pattern showing diffraction intensity maxima at 1/3 and 2/3 $\{112\}_\beta$ positions. With minimal oxygen present, ellipsoid shaped ω phase is observed, which is characteristic of the low misfit Ti-Nb system [38]. However, dark-field TEM (DF-TEM) images for higher oxygen levels (4.8 at. % O) show ω precipitates with a more elongated shape and higher number density compared to those at minimal oxygen levels (**Fig. 3c-d**). The evolution of the microstructure up to 31 days of ageing is illustrated in **Fig. 4** for different oxygen contents: 0.1, 1.5, 2.7, 3.4, and 4.1 at. % O. The elongated rod shape of ω precipitates initially observed at high oxygen contents is preserved at longer ageing times (**Fig. 4a-b, g**). Additionally, the increased number density of ω precipitates with elevated oxygen content compared to minimal oxygen is also retained. After 6 days of ageing, ω precipitates continued to grow in size (**Fig. 4g-j**). Precipitation of α laths (about 500 nm in length) is also seen in the 4.1 at. % O condition (**Fig. 4f**). The SAED pattern in this region confirms the presence of both ω and α phase at this oxygen level, with distinct reflections at the 1/2 $\{112\}_\beta$ positions corresponding to α.

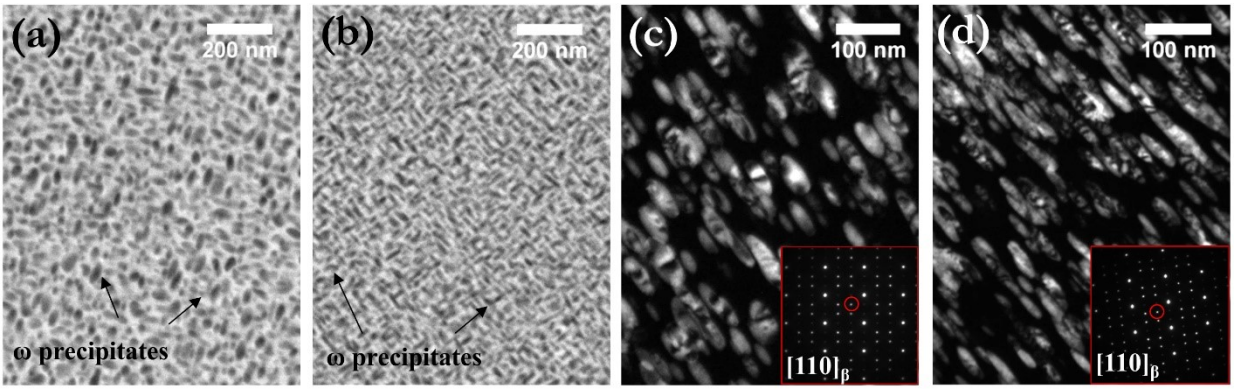

Fig. 3. SEM-BSE images for (a) DA Ti-20Nb with 0.1 at. % O and (b) OXA Ti-20Nb with 4.8 at. % O aged for 2 h at 450 °C. SAED pattern from $[110]_\beta$ zone axis and DF-TEM images using reflection in red circle from (c) DA Ti-20Nb aged for 2 h at 450°C with 0.1 at. % O, showing ellipsoidal ω precipitates, and (d) OXA Ti-20Nb aged for 2 h at 450 °C with 4.8 at. % O, showing elongated rod shaped ω precipitates and a higher precipitate number density.

Prolonged ageing of DA and OXA samples revealed differences in the α nucleation rate with varying oxygen content (**Fig. 4k-o**). After 22 d of ageing, microstructures observed in backscatter SEM images show that regions with the highest oxygen contents (3.4, 4.1 at. % O) contain significant numbers of α precipitates (~500 nm length) with some ω particles. With minimal oxygen content (0.1 at. % O), a similar microstructure is also observed, but the α laths are larger (~1 μm length) and nucleated in larger packets of similar orientation. Interestingly, regions with intermediate levels of oxygen (2.7 at. % O) show primarily ellipsoidal ω phase and a small number of α precipitates. Investigation of OXA samples after 31 d of ageing (**Fig. 4p-s**) shows that α phase does eventually nucleate in these high oxygen regions, but a significant amount of ω persists in the microstructure, in contrast with specimens containing 0.1 at. % O after 31 d of ageing (**Fig. 4t**) showing a large number of α laths. Furthermore, the ω phase observed at 1.5 at. % O has grown to ~400-500 nm in size, with some precipitates attaching together after 31 d of ageing (**Fig. 4s**). This attachment resulted in the formation of highly irregular precipitate chains that were distributed throughout the microstructure.

Aged microstructures revealed that oxygen levels seemed to influence ω number density. In an attempt to quantify the ω area fraction (used as a measure of phase fraction), SEM-BSE images for Ti-20Nb aged for 1, 6, and 14 days at 450 °C with 0.1 or 3.4 at. % O were segmented

using binary histogram-based thresholding (**Fig. 5**). The ω area fraction showed some variation depending on the specific field of view, but regardless of oxygen content ranged from approximately 44-48 %. Therefore, the phase fraction of ω with different oxygen contents was relatively constant across ageing times studied here. However, qualitative differences in the distribution of ω phase (relating to number density) with oxygen level are clearly observed, and microstructures for 3.4 at. % O are consistently more refined than those with minimal oxygen. The most significant difference for ω distributions is observed for Ti-20Nb specimens aged for 14 days at 450 °C (**Figs. 5c, 5f**), with finer ω precipitates, and consequently increased number density, seen with the elevated oxygen content.

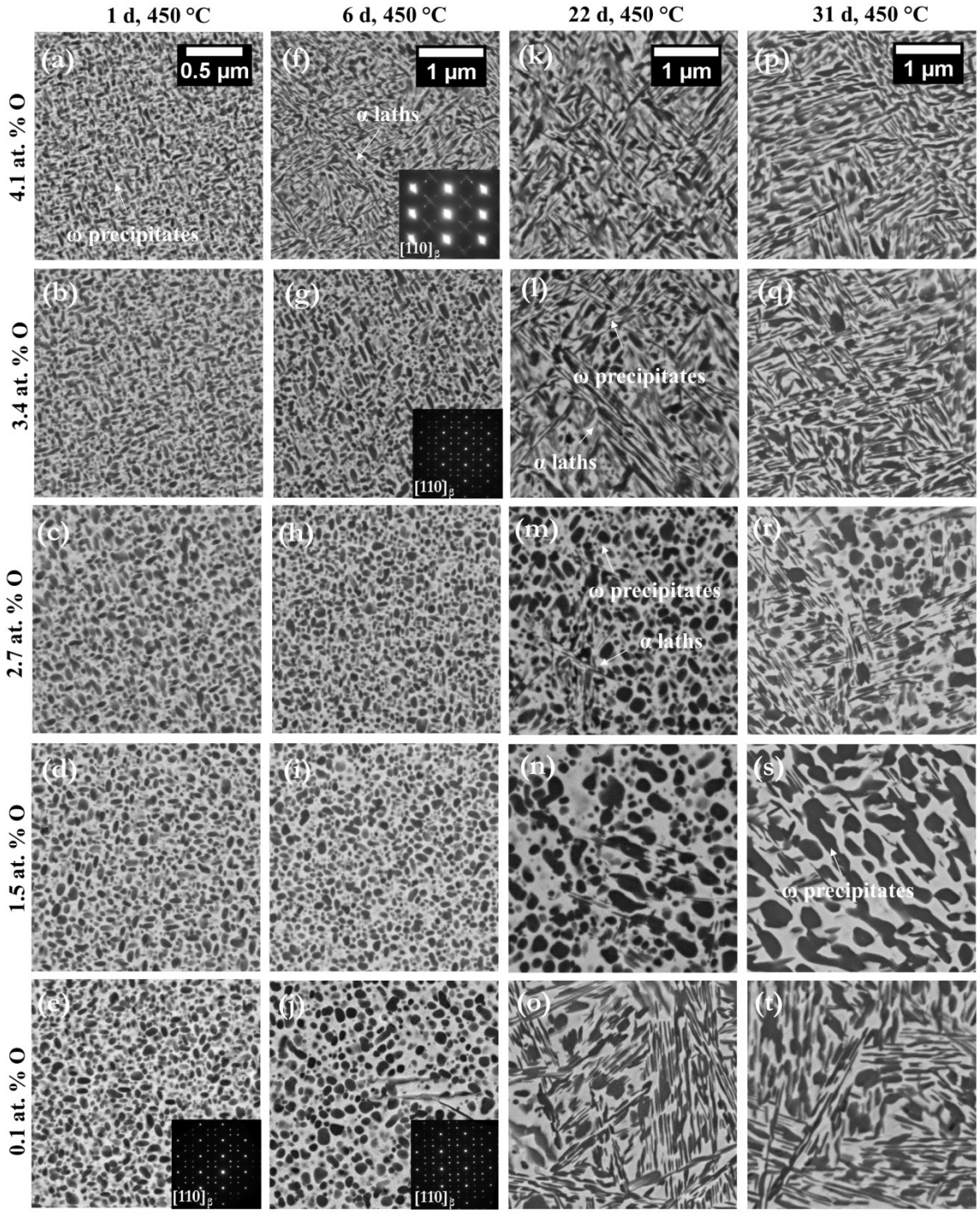

Fig. 4. SEM-BSE images from OXA and DA Ti-20Nb aged at 450 °C corresponding to different oxygen contents: 0.1, 1.5, 2.7, 3.4, 4.1 at. % O. Microstructural images correspond to isothermal ageing after (a-e) 1 day, (f-j) 6 days, (k-o) 22 days, and (p-t) 31 days. Insets of TEM SAED patterns were taken from the $[110]_\beta$ zone axis.

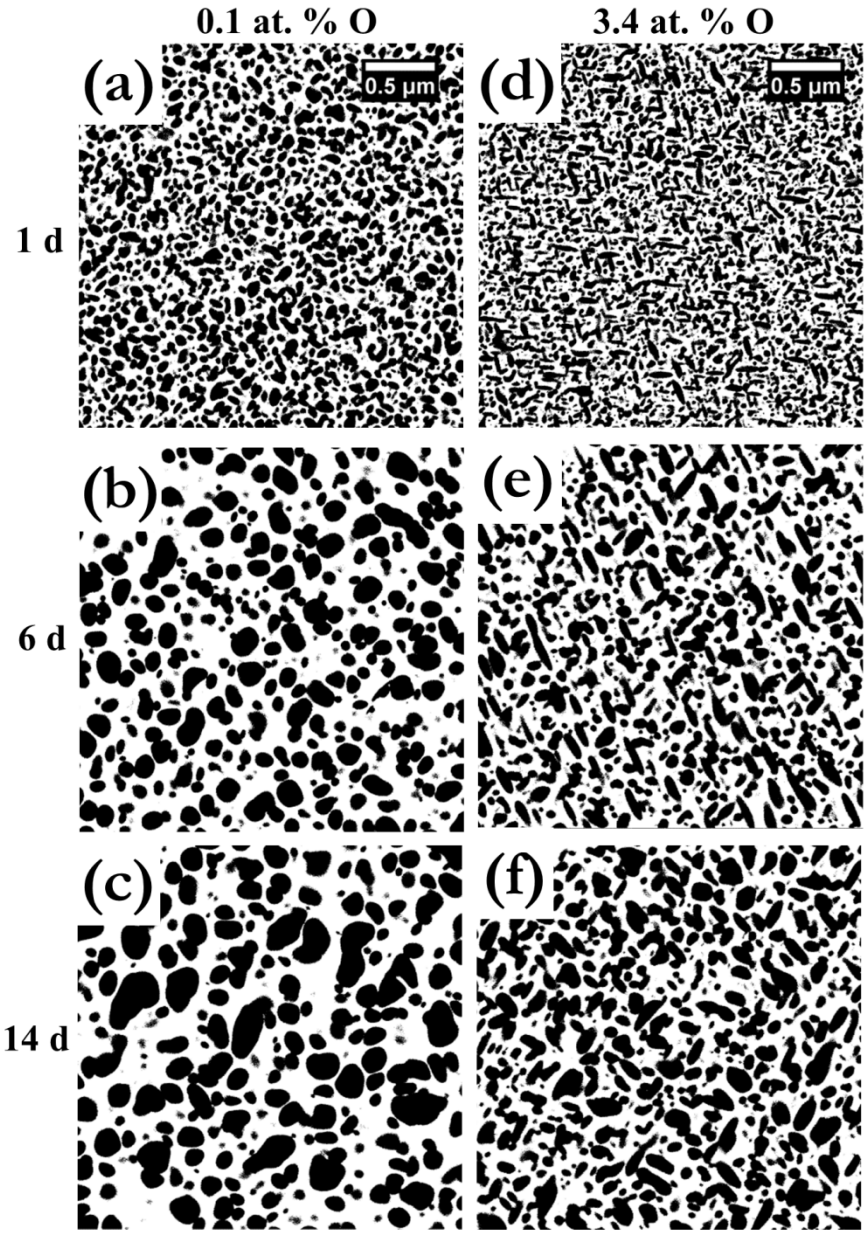

Fig. 5. SEM-BSE images segmented using binary histogram-based thresholding for the ω phase in aged Ti-20Nb at 450 °C in the following conditions: (a) 0.1 at. % O for 1 d, (b) 0.1 at. % O for 6 d, (c) 0.1 at. % O for 14 d, (d) 3.4 at. % O for 1 d, (e) 3.4 at. % O for 6 d, and (f) 3.4 at. % O for 14 d.

The β + ω microstructure after 6 days of ageing examined by dark-field TEM imaging shows the change in ω precipitate shape with oxygen in greater detail (**Fig. 6**). With very little oxygen present, the ellipsoid ω phase has a major axis along the $<111>_{\beta}$ direction [5] and a

maximum size of ~150 nm. At 3.4 at. % O, the ω phase shows additional lengthening along <111>$_\beta$ to form an elongated rod shape. The maximum observed major axis is roughly 300 nm. Aspect ratio measurements from the TEM dark-field data confirm the additional shape anisotropy for ω with higher oxygen (3.4 at. % O: up to 4.2 to 1 aspect ratio) compared to minimal oxygen (0.1 at. % O: 1.5 to 1 aspect ratio). 3D FIB tomography collected after 6 days of ageing with 3.4 at. % O clearly demonstrates that the additional lengthening is constrained to one direction to form a rod (**Fig. 7**).

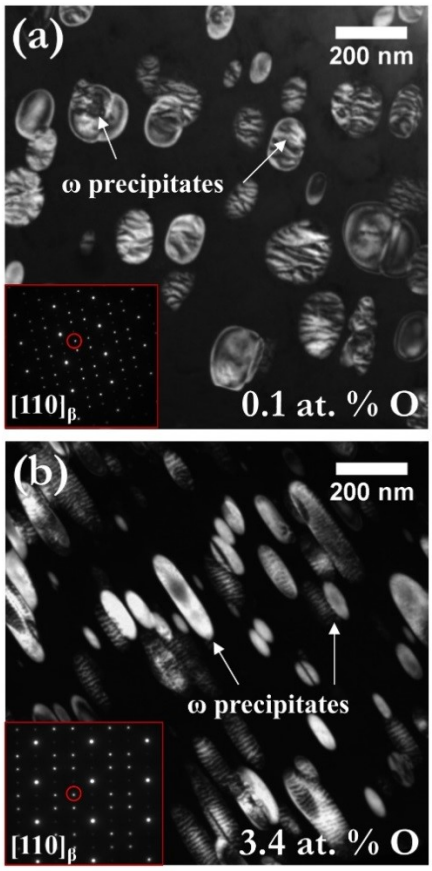

Fig. 6. SAED pattern from [110]$_\beta$ zone axis and DF-TEM image using reflection in red circle from (a) DA Ti-20Nb with 0.1 at. % O aged for 6 days at 450 °C, showing ellipsoidal ω precipitates, and (b) OXA Ti-20Nb with 3.4 at. % O aged for 6 days at 450 °C, showing elongated rod shaped ω precipitates.

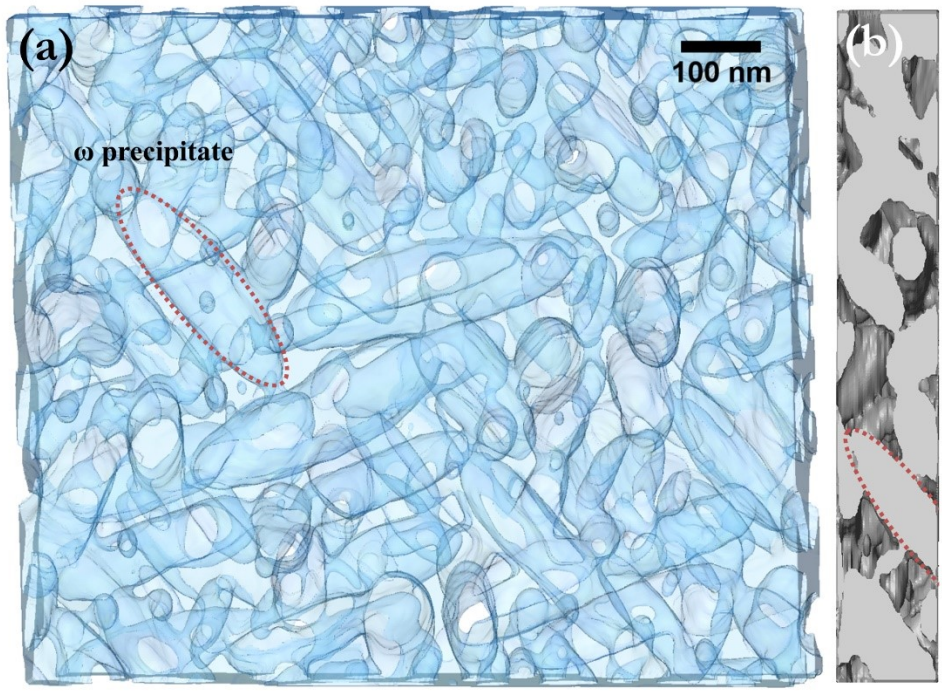

Fig. 7. (a) Front view and (b) side view of reconstructed dataset (970 by 820 by 130 nm) collected using FIB tomography from OXA Ti-20Nb with 3.4 at. % O aged for 6 days at 450 °C corresponding to microstructure in **Fig. 4g**. Red dotted line outlines an example of a rod shaped ω precipitate.

In order to quantify the oxygen partitioning behavior with respect to β and ω during ageing, atom probe tomography was conducted on an OXA specimen after 6 d of ageing at 450 °C with 3.4 at. % O (corresponding to microstructure in **Fig. 4g** and **Fig. 7**). The reconstructed APT dataset (**Fig. 8**) shows Nb depleted and O enriched regions corresponding to ω phase and Nb enriched regions corresponding to the β matrix. A proximity histogram (or proxigram) that represents a concentration profile as a function of distance from the β/ω interface was generated using an iso-concentration surface of 63 at. % Ti (**Fig. 8b-c**) and shows that the ω phase is rich in O and Ti, but not in Nb. Additionally, very little oxygen is measured in the β phase. Based on uniform values of the proxigram, the ω and β compositions are measured as follows: ω – Nb: 3 at. %, O: 6 at. %, Ti: Balance, β – Nb: 28 at. %, O: 0.3 at. %, Ti: Balance. Thus, oxygen partitions to ω precipitates and Nb partitions to the β matrix during ageing, as previously reported by Niinomi et al. [22].

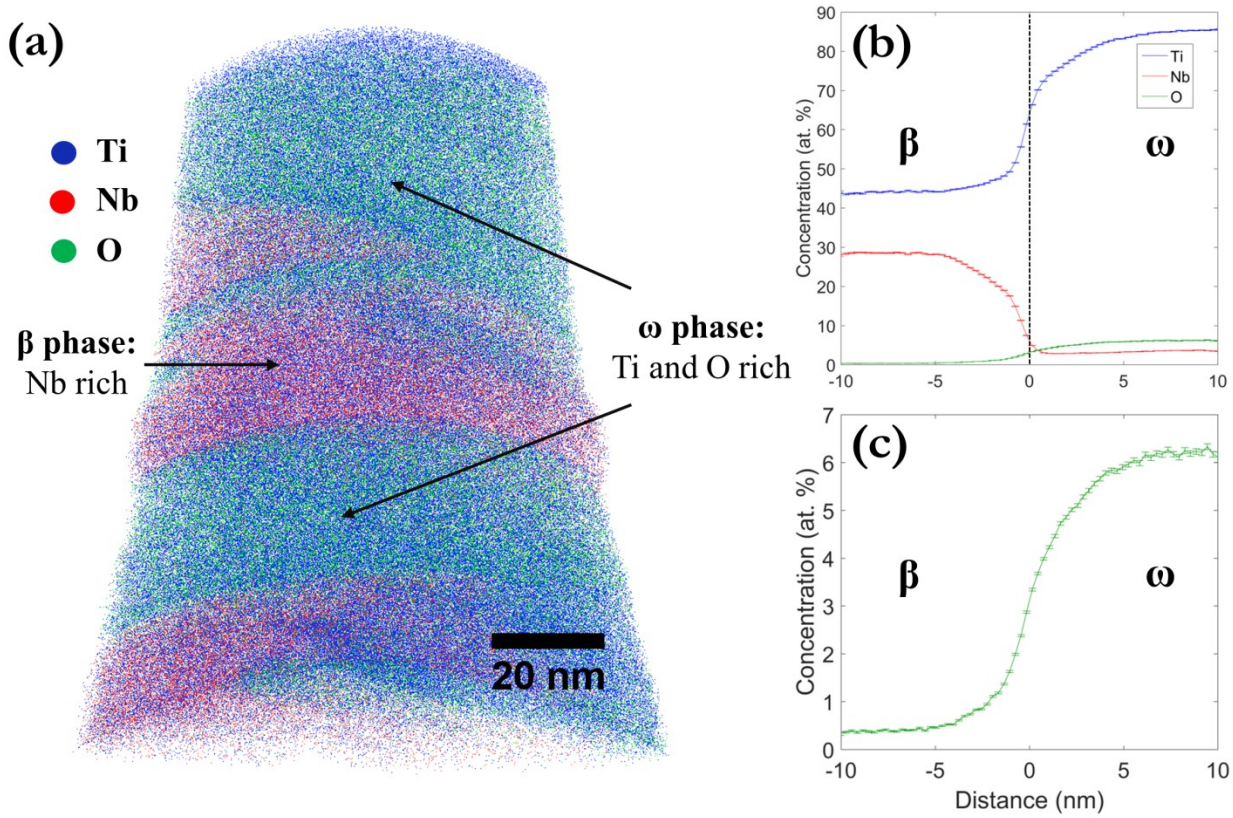

Fig. 8. (a) APT reconstruction of sample from OXA Ti-20Nb with 3.4 at. % O aged for 6 days at 450 °C. Proxigram showing concentration profile for (b) Ti, Nb, and (c) O as a function of distance from the β/ω interface using 63 at. % Ti iso-concentration surfaces.

3.3 Two-step ageing at 450 °C and 600 °C

A two-step ageing experiment was conducted to investigate the extent of ω phase stability with oxygen. A set of DA and OXA samples with 3 d of ageing at 450 °C were subsequently aged for 1 h at 600 °C to promote ω dissolution and faster α formation. The ω solvus for pure Ti is reported to be 485 °C [3], therefore ω is not expected to be stable at 600 °C. After two-step ageing, SEM backscatter images show that the resulting microstructures also strongly depend on oxygen content (**Fig. 9**). At low oxygen contents (0.1, 1.5 at. % O), martensite formation is observed with few α precipitates (**Fig. 9b**). As the oxygen content increases (3.6 at. % O), α precipitates appear to have nucleated in patches, with ω-like particles at the center of the patches (**Fig. 9c**). Finally, at the highest levels of oxygen (4.1-4.8 at % O), dense distributions of α laths and ω-like particles are observed throughout the microstructure

(**Fig. 9d**). TEM SAED patterns in the 4.8 at. % O region (**Fig. 9e**) show both ω and α reflections and confirm the co-existence of these phases [39, 40].

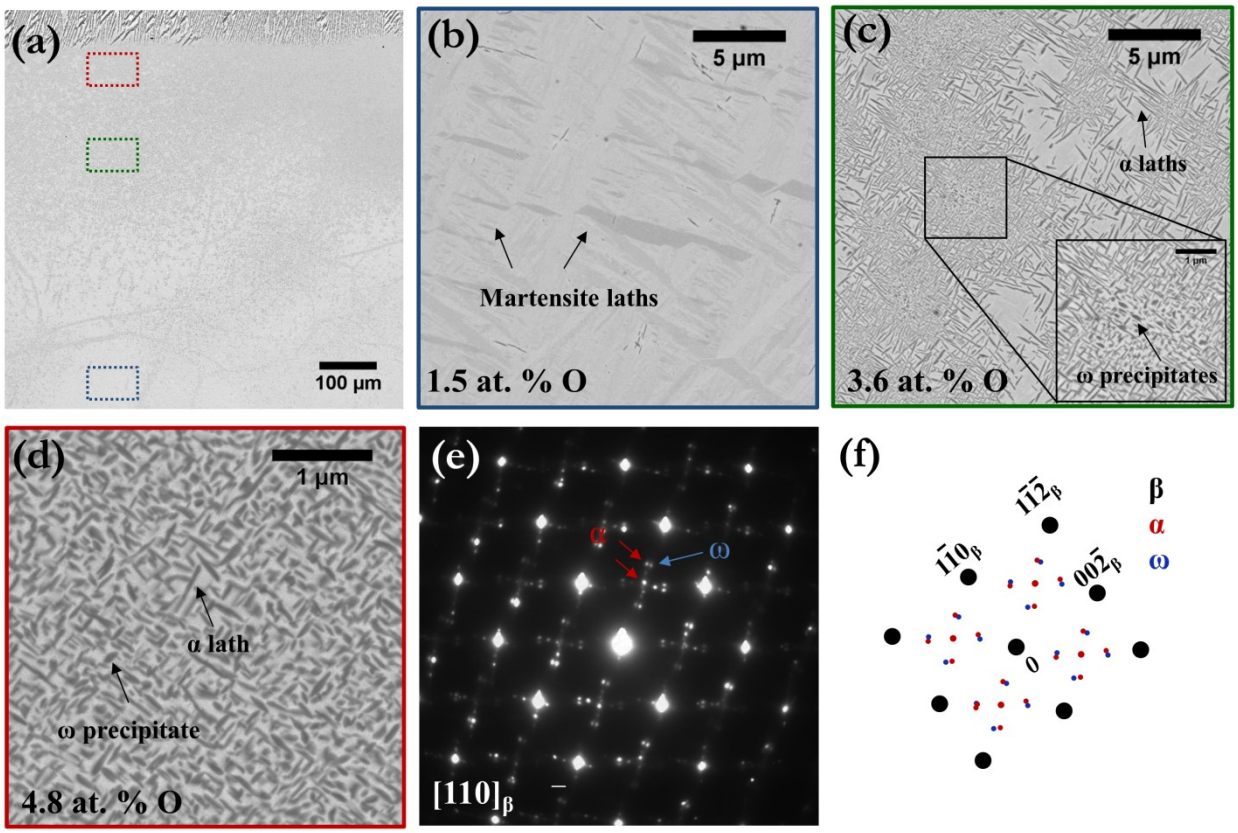

Fig. 9. SEM-BSE images from OXA Ti-20Nb aged using a two-step heat treatment for 3 d at 450 °C and 1 h at 600 °C. (a) Low magnification image of cross section. (b) Microstructure from region in blue box of low magnification image with 1.5 at. % O showing martensite and small α precipitates. (c) Microstructure from region in green box of low magnification image with 3.6 at. % O showing ω and α precipitate patches. (d) Microstructure and (e) SAED pattern with (f) key diagram from $[110]_\beta$ zone axis from region in red box of low magnification image with 4.8 at. % O showing ω and α precipitates.

4. Discussion

The results reveal that oxygen content significantly affects ω and α precipitation in a non-linear manner in the β matrix of Ti-20Nb. Elevated oxygen content results in a rod-like precipitate shape and higher number density of the ω phase. With additional ageing, these shape

and number density differences were preserved, and ω showed a slower growth rate with high oxygen. Prolonged ageing yielded α precipitation at all observed oxygen contents, but the rate and amount of α nucleation was heavily influenced by the level of oxygen. The slowest α nucleation rate was observed with intermediate levels of oxygen in solid solution (2.7 at. % O) compared to faster precipitation with minimal (0.1 at. %) and elevated (4.1 at. %) oxygen. Below we discuss the effects of oxygen on ω and α precipitation and phase stability.

4.1 Role of oxygen on martensite formation and ω nucleation

Previous studies [11, 12, 41] have shown that oxygen in solid solution (0.5 at. % or greater) suppresses martensite formation during quenching in Ti-Nb alloys. However, the present results (**Fig. 2**) with up to about 5 at. % O suggest that martensite suppression depends on both Nb and O content and may not be suppressed with oxygen if it is sufficiently stabilized at lower Nb contents. Oxidation of Ti-20Nb specimens resulted in a gradient of oxygen concentration in the matrix from the surface to center of specimens, and precipitation of large α laths in the subsurface metal just below the oxide layer is consistent with oxygen stabilizing the α phase. Martensite formation was confirmed in the β matrix below the α + β region upon quenching after oxidation (**Fig. 2b**). Additionally, at higher Nb contents, martensite formation was suppressed in the matrix with high oxygen. This is shown in the β matrix between α laths in the two-phase α + β region of **Fig. 2a** where the Nb and O contents were measured using WDS as roughly 23 at. % and 4.9 at. %, respectively. The suppression of martensite with oxygen in literature has been attributed to different factors, including an increase in the energy barrier of the transformation and formation of a semi-α" structure that acts as local barriers to long range martensite formation [42], a change in the relative stability of β and α" [43], and the presence of oxygen atoms in octahedral sites inhibiting contraction along the a-axis of α" martensite [44]. However, most previous studies were conducted with Nb content between 23-25 at. %, corresponding to a martensite start temperature (T_m) of roughly 100 °C [3]. Clearly, 1 at. % O is able to suppress martensite formation at these Nb compositions [11]. In Ti-20Nb used in this study with a T_m of about 200 °C [3], even approximately 5 at. % O, corresponding to the oxygen level measured at the (α lath + β) / β matrix interface where martensite formation was observed (**Fig. 2**), was not enough to suppress martensite formation. Similarly, a Ti-11Nb-4O at. % alloy fabricated through powder metallurgy also showed minor α" formation after solution treatment [45]. Curiously, Ti

alloys with the same 20 at. % Nb content have been reported to suppress martensite formation with only 0.7 at. % O in solid solution [46].

Upon aging, the ω precipitate number density increased with greater oxygen content (**Fig. 3a-b**). A simple thermodynamic basis for this observation may be attributed to oxygen increasing the phase stability of ω. According to published metastable Ti-Nb phase diagrams [3], the alloy composition and ageing temperature used in this study are to the right of the $T_0^{\beta/\omega}$ line that defines equality of the β and ω Gibbs free energies. Therefore, in the absence of oxygen, ω is expected to form by nucleation and growth. If additions of oxygen increase the phase stability of ω (i.e. lowering its Gibbs free energy), it consequently also increases the driving force for ω nucleation, leading to a higher precipitate number density, as experimentally observed. Increases in ω phase stability with oxygen may also shift the ω Gibbs free energy curve such that the alloy concentration moves to the left of the $T_0^{\beta/\omega}$ line. There, a displacive transformation from β to ω, in which $\{111\}_\beta$ atomic planes partially collapse to form ω-like embryos [47, 48], becomes possible, resulting in an increased ω precipitation rate.

4.2 Role of oxygen on ω precipitate morphology and growth rate

Growth and coarsening of isothermal ω during ageing require significant diffusion, with Nb being rejected from the ω phase and diffusing in the β matrix to the equilibrium composition. During ageing, oxygen partitions to ω from the β matrix, as previously shown [22, 23] and further confirmed by the present APT measurements (**Fig. 8**). The influence of oxygen content on the growth rate and morphology of the ω precipitates (**Fig. 5, 6**) may stem from changes in the nature of the interface, the structure of the ω phase, and/or from kinetic limitations associated with solute diffusion and the β to ω transformation.

Increasing the alloy's oxygen concentration led to the formation of rod shaped ω precipitates with increased aspect ratio compared to ellipsoidal shapes with minimal oxygen (**Figs. 4, 6**). Rod shaped ω phase at small sizes has been reported in literature [25, 49] and also observed in this study (**Fig. 3d**). Larger rod-like ω in a β Ti alloy processed with rapid heating rates and short ageing times has been shown [50], but the well-developed size of rod shaped ω that persists with long ageing times greater than 6 days (**Fig. 6b**) has not been reported previously. If one assumes local equilibrium, precipitate shape is classically governed by the balance between interfacial energy and elastic misfit strain contributions. Density functional

theory (DFT) calculations on low energy configurations of the ω/β interface suggested that the ellipsoidal shape in oxygen-free Ti-Nb may be attributed to interfacial energy anisotropy [51] and traditionally, the ellipsoidal shape has been associated with low misfit Ti alloy systems [38]. The retention of an ellipsoid shape for Ti-Nb-O ω precipitates suggests that interfacial energy may still play some role in controlling precipitate shape. However, the increase in aspect ratio to form a rod shape suggests that misfit strains through lattice distortion with added oxygen may also be relevant. Moreover, beyond equilibrium growth, precipitate shape may be affected by kinetic effects, in which the β to ω transformation favors a particular direction or orientation during growth.

Conflicting or lack of literature results on equilibrium contributions complicates the current understanding of the role of O on ω growth rate. Without oxygen present, the nature of the ω/β interface reportedly evolves during ageing, and these structural changes may alter the influence of this interface on controlling ω growth. The nanoscale ω phase that forms upon quenching has been reported as coherent with a diffuse interface [47]. However, as ω grows during ageing, a sharp interface [47] has been observed with the existence of ledges [25, 39], suggesting that growth could be interface-limited. During growth, the ω/β interfacial character may also change to semi-coherent [25], and misfit dislocations have been reported when ω has reached ~200 nm in size [52]. In contrast, it is well known that diffusion and rejection of β-stabilizers occurs during isothermal ω growth [1], and early literature suggested diffusion-controlled ω nucleation and growth for Ti-Mo alloys [53]. With oxygen, additional contributions to ω growth rate may arise from kinetic effects. As discussed above, the transformation from β to ω may happen very quickly by plane collapse, as a consequence of the oxygen stabilization of ω with respect to the β phase. As highlighted in [18], oxygen may increase the energy barrier associated with this collapse, and consequently reduce the rate of the transformation. A similar increase in energy barrier with oxygen that is expected to reduce nucleation rate has been shown for the martensitic α to ω transformation that takes place at high pressures [54], and ω suppression with oxygen has been experimentally verified for this transformation [55]. Kinetic limitations relating to high activation energy barrier for the β to ω transformation during nucleation have also been recently reported in the Ti-V system [56]. In the present results, the β to ω transformation is not suppressed with oxygen, likely due to the relatively high ageing temperature that allows for substantial diffusion, but the increase in energy barrier may slow the

transformation rate during ω growth, as observed experimentally (**Fig. 5**). Since O prefers the octahedral sites on $\{111\}_\beta$ planes, the β to ω transformation involving collapsing O atoms, which accounts for three out of four transformation pathways, requires short displacements for O to relocate to its final site and are associated with a 30-40 meV/atom energy barrier [18]. Such a high energy barrier would kinetically slow down the β to ω transformation and therefore the ω growth rate.

4.3 Role of oxygen on α nucleation in the presence of ω

With interstitial oxygen in the β matrix, prolonged isothermal ageing revealed that α eventually precipitated at all oxygen levels in this study (0.1-4.1 at. % O), which is consistent with ω being a metastable phase in β Ti alloys [52]. Furthermore, oxygen increases the energy of ω relative to that of α [54]. Surprisingly, α nucleation in Ti-Nb was quite slow, and ω persisted for significantly longer ageing periods in specimens both with and without oxygen. Literature reports on the effects of oxygen are conflicting, with oxygen having been reported as either reducing [22] or accelerating [19, 20] the rate of α precipitation from ω. Interestingly, the α precipitation rate in the presence of the ω phase was observed to be slowest for intermediate levels of oxygen (2.7 at. %). Oxygen is a potent α-stabilizer [1], which explains the early α nucleation at relatively high oxygen levels (3.4, 4.1. at. % O). Nonetheless, the formation of ω prior to α suggests that α nucleation from β is associated with a high energy barrier and may be facilitated by ω nucleation. α nucleates at later times in oxygen-free samples and α nucleation is most delayed at intermediate levels of oxygen. Based on these results, we hypothesize that small levels of oxygen increase the ω phase stability with respect to the β phase without significantly increasing α stability, while higher levels of oxygen dramatically increase α stability over that of the ω phase. These stability changes would result in differences in the α nucleation driving force that account for the observed changes in precipitation rate. Two-step ageing results (**Fig. 9**) also suggest that elevated oxygen helps to expand the region of ω phase stability to higher temperatures. During the second ageing step at 600 °C, which is above the reported ω solvus [3], Nb and Ti diffusion is expected to dissolve the ~200 nm ω phase that precipitated during the first ageing step at 450 °C [57]. This dissolution was observed in both DA specimens and the center of OXA specimens with lower oxygen content, and martensite is formed in these regions upon quenching. However, at the highest interstitial oxygen contents (4.8 at. %), ω and α were

identified using electron diffraction, indicating that the elevated oxygen content helped to stabilize the ω phase even at 600 °C. These insights on oxygen as both an α and ω-stabilizer may open new avenues of microstructural control for future design and development of β-Ti alloys.

5. Conclusions

The nucleation and growth of ω and α precipitates in Ti-20 at. % Nb with 0.1-4.8 at. % O was systematically investigated during isothermal ageing to elucidate oxygen effects on phase transformations in metastable β Ti alloys. The main conclusions are as follows:

1. Oxidation experiments were used to investigate a range of oxygen contents in solid solution between 0.1 to 4.8 at. % on the subsequent ageing behavior of β titanium alloys.
2. Ti-20Nb specimens with oxygen levels up to about 5 at. % showed martensite formation upon quenching following oxidation exposure. Therefore, the ability of oxygen to suppress martensite formation in metastable β Ti depends on both Nb and O content.
3. Oxygen increases the stability of ω phase. During ageing, ω number density increases with elevated oxygen. Additionally, oxygen induces ω precipitates to form with a rod-like shape compared to an ellipsoid shape without oxygen present. Elevated oxygen content also expands the region of ω phase stability up to 600 °C, indicating that oxygen is an ω-stabilizer in β Ti alloys.
4. Oxygen partitions to the ω phase during ageing and the growth rate of ω with high oxygen was slowed compared to ω formed with minimal oxygen. This growth rate change is attributed to an increased energy barrier for the β to ω transformation with oxygen. Thus, oxygen shows a dual effect on the ω phase by increasing phase stability but kinetically limiting the rate of transformation from β.
5. α nucleation in the presence of ω depends on oxygen content. With high oxygen (greater than 3.4 at. % O), α precipitates at the fastest rate due to the significant increase in α thermodynamic phase stability and nucleation driving force with elevated oxygen. With intermediate levels of oxygen (2.7 at. %), α forms at the slowest rate due to a reduced nucleation driving force from increased ω phase stability, but relatively unchanged α stability. Therefore, oxygen content allows for microstructural control of ω and α transformation rates in β titanium alloys.

Acknowledgements

This material is based upon work supported by the National Science Foundation (NSF) through grants NSF DMR-1436154 and CMMI-1729166, and the Graduate Research Fellowship Program under grant No. DGE 1256260. The authors gratefully acknowledge financial and technical support from the University of Michigan Center for Materials Characterization and Robert B. Mitchell Electron Microbeam Analysis Lab. The authors would also like to thank Dr. John Foltz, Dr. Owen Neill, Dr. Anton Van der Ven, Harsha Gunda, and Dr. Dallas Trinkle for providing the Ti-20Nb button, experimental assistance with WDS, and discussions on α and ω phase stability.

References

[1] D. Banerjee, J.C. Williams, Perspectives on Titanium Science and Technology, Acta Materialia 61(3) (2013) 844-879.
[2] C. Leyens, M. Peters, Beta Titanium Alloys, in Titanium and Titanium Alloys: Fundamentals and Applications, Wiley-VCH Verlag GmbH & Co. KGaA, Weinheim, FRG, 2003, pp. 37-57.
[3] M. Bönisch, A. Panigrahi, M. Calin, T. Waitz, M. Zehetbauer, W. Skrotzki, J. Eckert, Thermal stability and latent heat of Nb–rich martensitic Ti-Nb alloys, Journal of Alloys and Compounds 697 (2017) 300-309.
[4] R. Kolli, A. Devaraj, A Review of Metastable Beta Titanium Alloys, Metals 8(7) (2018) 506.
[5] S. Banerjee, R. Tewari, G.K. Dey, Omega phase transformation – morphologies and mechanisms, International Journal of Materials Research 97(7) (2006) 963-977.
[6] J.D. Cotton, R.D. Briggs, R.R. Boyer, S. Tamirisakandala, P. Russo, N. Shchetnikov, J.C. Fanning, State of the Art in Beta Titanium Alloys for Airframe Applications, JOM 67(6) (2015) 1281-1303.
[7] A. Biesiekierski, J. Wang, M.A. Gepreel, C. Wen, A new look at biomedical Ti-based shape memory alloys, Acta biomaterialia 8(5) (2012) 1661-9.
[8] M. Niinomi, M. Nakai, J. Hieda, Development of new metallic alloys for biomedical applications, Acta biomaterialia 8(11) (2012) 3888-903.
[9] Z. Liu, G. Welsch, Effects of oxygen and heat treatment on the mechanical properties of alpha and beta titanium alloys, Metallurgical Transactions A 19(3) (1988) 527-542.
[10] T. Saito, T. Furuta, J.H. Hwang, S. Kuramoto, K. Nishino, N. Suzuki, R. Chen, A. Yamada, K. Ito, Y. Seno, T. Nonaka, H. Ikehata, N. Nagasako, C. Iwamoto, Y. Ikuhara, T. Sakuma, Multifunctional Alloys Obtained via a Dislocation-Free Plastic Deformation Mechanism, Science 300(5618) (2003) 464-7.
[11] M. Tahara, H.Y. Kim, T. Inamura, H. Hosoda, S. Miyazaki, Lattice modulation and superelasticity in oxygen-added β-Ti alloys, Acta Materialia 59(16) (2011) 6208-6218.
[12] M. Besse, P. Castany, T. Gloriant, Mechanisms of deformation in gum metal TNTZ-O and TNTZ titanium alloys: A comparative study on the oxygen influence, Acta Materialia 59(15) (2011) 5982-5988.

[13] P. Castany, A. Ramarolahy, F. Prima, P. Laheurte, C. Curfs, T. Gloriant, In situ synchrotron X-ray diffraction study of the martensitic transformation in superelastic Ti-24Nb-0.5N and Ti-24Nb-0.5O alloys, Acta Materialia 88 (2015) 102-111.
[14] L.S. Wei, H.Y. Kim, T. Koyano, S. Miyazaki, Effects of oxygen concentration and temperature on deformation behavior of Ti-Nb-Zr-Ta-O alloys, Scripta Materialia 123 (2016) 55-58.
[15] L.S. Wei, H.Y. Kim, S. Miyazaki, Effects of oxygen concentration and phase stability on nano-domain structure and thermal expansion behavior of Ti–Nb–Zr–Ta–O alloys, Acta Materialia 100 (2015) 313-322.
[16] M. Ikeda, S.-y. Komatsu, T. Sugimoto, K. Kamei, Influence of Oxygen Content on Electrical Resistivity and Phase Constitution in Quenched Ti-V Alloys, Journal of the Japan Institute of Metals 55(3) (1991) 260-266.
[17] N.E. Paton, J.C. Williams, The influence of oxygen content on the athermal β-ω transformation, Scripta Metallurgica 7(6) (1973) 647-649.
[18] J.G. Niu, D.H. Ping, T. Ohno, W.T. Geng, Suppression effect of oxygen on the β to ω transformation in a β-type Ti alloy: insights from first-principles, Modelling and Simulation in Materials Science and Engineering 22(1) (2014) 015007.
[19] J.C. Williams, B.S. Hickman, D.H. Leslie, The effect of ternary additions on the decomposition of metastable beta-phase titanium alloys, Metallurgical Transactions 2(2) (1971) 477-484.
[20] J.I. Qazi, B. Marquardt, L.F. Allard, H.J. Rack, Phase transformations in Ti–35Nb–7Zr–5Ta–(0.06–0.68)O alloys, Materials Science and Engineering: C 25(3) (2005) 389-397.
[21] M. Tane, T. Nakano, S. Kuramoto, M. Hara, M. Niinomi, N. Takesue, T. Yano, H. Nakajima, Low Young's modulus in Ti–Nb–Ta–Zr–O alloys: Cold working and oxygen effects, Acta Materialia 59(18) (2011) 6975-6988.
[22] M. Niinomi, M. Nakai, M. Hendrickson, P. Nandwana, T. Alam, D. Choudhuri, R. Banerjee, Influence of oxygen on omega phase stability in the Ti-29Nb-13Ta-4.6Zr alloy, Scripta Materialia 123 (2016) 144-148.
[23] T. Homma, A. Arafah, D. Haley, M. Nakai, M. Niinomi, M.P. Moody, Effect of alloying elements on microstructural evolution in oxygen content controlled Ti-29Nb-13Ta-4.6Zr (wt%) alloys for biomedical applications during aging, Materials Science and Engineering: A 709 (2018) 312-321.
[24] T. Li, D. Kent, G. Sha, L.T. Stephenson, A.V. Ceguerra, S.P. Ringer, M.S. Dargusch, J.M. Cairney, New insights into the phase transformations to isothermal ω and ω-assisted α in near β-Ti alloys, Acta Materialia 106 (2016) 353-366.
[25] T. Li, D. Kent, G. Sha, H. Liu, S.G. Fries, A.V. Ceguerra, M.S. Dargusch, J.M. Cairney, Nucleation driving force for ω-assisted formation of α and associated ω morphology in β-Ti alloys, Scripta Materialia 155 (2018) 149-154.
[26] Y. Zheng, R.E.A. Williams, D. Wang, R. Shi, S. Nag, P. Kami, J.M. Sosa, R. Banerjee, Y. Wang, H.L. Fraser, Role of ω phase in the formation of extremely refined intragranular α precipitates in metastable β-titanium alloys, Acta Materialia 103 (2016) 850-858.
[27] Y. Zheng, R.E.A. Williams, J.M. Sosa, T. Alam, Y. Wang, R. Banerjee, H.L. Fraser, The indirect influence of the ω phase on the degree of refinement of distributions of the α phase in metastable β-Titanium alloys, Acta Materialia 103 (2016) 165-173.

[28] S.A. Mantri, D. Choudhuri, T. Alam, G.B. Viswanathan, J.M. Sosa, H.L. Fraser, R. Banerjee, Tuning the scale of α precipitates in β-titanium alloys for achieving high strength, Scripta Materialia 154 (2018) 139-144.
[29] M.J. Lai, T. Li, D. Raabe, ω phase acts as a switch between dislocation channeling and joint twinning- and transformation-induced plasticity in a metastable β titanium alloy, Acta Materialia 151 (2018) 67-77.
[30] S.A. Mantri, D. Choudhuri, T. Alam, V. Ageh, F. Sun, F. Prima, R. Banerjee, Change in the deformation mode resulting from beta-omega compositional partitioning in a Ti Mo alloy: Room versus elevated temperature, Scripta Materialia 130 (2017) 69-73.
[31] H. Liu, M. Niinomi, M. Nakai, K. Cho, H. Fujii, Deformation-induced ω-phase transformation in a β-type titanium alloy during tensile deformation, Scripta Materialia 130 (2017) 27-31.
[32] F. Sun, J.Y. Zhang, P. Vermaut, D. Choudhuri, T. Alam, S.A. Mantri, P. Svec, T. Gloriant, P.J. Jacques, R. Banerjee, F. Prima, Strengthening strategy for a ductile metastable β-titanium alloy using low-temperature aging, Materials Research Letters 5(8) (2017) 547-553.
[33] J. Gao, A.J. Knowles, D. Guan, W.M. Rainforth, ω phase strengthened 1.2GPa metastable β titanium alloy with high ductility, Scripta Materialia 162 (2019) 77-81.
[34] J.J. Donovan, D. Kremser, J. Fournelle, K. Goermann, Probe For EPMA v.12.6.3 User's Guide and Reference. Xtreme Edition, Eugene, OR, 2019, p. 431.
[35] D.A.S. J.J. Donovan, M.L. Rivers, An Improved Interference Correction for Trace Element Analysis, Microbeam Analysis 2 (1993) 23-28.
[36] J.I. Goldstein, S.K. Choi, F.J.J. Van Loo, H.J.M. Heijligers, G.F. Bastin, W.G. Sloof, The influence of oxide surface layers on bulk electron probe microanalysis of oxygen-application to Ti-Si-O compounds, Scanning 15(3) (1993) 165-170.
[37] Z. Liu, G. Welsch, Literature Survey on Diffusivities of Oxygen, Aluminum, and Vanadium in Alpha Titanium, Beta Titanium, and in Rutile, Metallurgical Transactions A 19(4) (1988) 1121-1125.
[38] M.J.B. J.C. Williams, The Influence of Misfit on the Morphology and Stability of the Omega Phase in Titanium-Transition Metal Alloys, Transactions of the Metallurgical Society of AIME 245 (1969) 2352-2355.
[39] Y. Zheng, D. Choudhuri, T. Alam, R.E.A. Williams, R. Banerjee, H.L. Fraser, The role of cuboidal ω precipitates on α precipitation in a Ti-20V alloy, Scripta Materialia 123 (2016) 81-85.
[40] M. Hendrickson, S.A. Mantri, Y. Ren, T. Alam, V. Soni, B. Gwalani, M. Styles, D. Choudhuri, R. Banerjee, The evolution of microstructure and microhardness in a biomedical Ti–35Nb–7Zr–5Ta alloy, Journal of Materials Science 52(6) (2016) 3062-3073.
[41] A. Ramarolahy, P. Castany, F. Prima, P. Laheurte, I. Peron, T. Gloriant, Microstructure and mechanical behavior of superelastic Ti-24Nb-0.5O and Ti-24Nb-0.5N biomedical alloys, Journal of the mechanical behavior of biomedical materials 9 (2012) 83-90.
[42] J.G. Niu, W.T. Geng, Oxygen-induced lattice distortion in β -Ti 3 Nb and its suppression effect on β to α ″ transformation, Acta Materialia 81 (2014) 194-203.
[43] R. Salloom, D. Reith, R. Banerjee, S.G. Srinivasan, First principles calculations on the effect of interstitial oxygen on phase stability and β–α″ martensitic transformation in Ti–Nb alloys, Journal of Materials Science 53(16) (2018) 11473-11487.
[44] C. Hammond, Orthorhombic martensites in titanium alloys, Scripta Metallurgica 6(7) (1972) 569-570.

[45] B. Yuan, B. Yang, Y. Gao, M. Lai, X.H. Chen, M. Zhu, Achieving ultra-high superelasticity and cyclic stability of biomedical Ti–11Nb–4O (at.%) alloys by controlling Nb and oxygen content, Materials & Design 92 (2016) 978-982.
[46] M. Tahara, T. Inamura, H.Y. Kim, S. Miyazaki, H. Hosoda, Role of oxygen atoms in α″ martensite of Ti-20 at.% Nb alloy, Scripta Materialia 112 (2016) 15-18.
[47] A. Devaraj, S. Nag, R. Srinivasan, R.E.A. Williams, S. Banerjee, R. Banerjee, H.L. Fraser, Experimental evidence of concurrent compositional and structural instabilities leading to ω precipitation in titanium–molybdenum alloys, Acta Materialia 60(2) (2012) 596-609.
[48] S. Nag, A. Devaraj, R. Srinivasan, R.E. Williams, N. Gupta, G.B. Viswanathan, J.S. Tiley, S. Banerjee, S.G. Srinivasan, H.L. Fraser, R. Banerjee, Novel mixed-mode phase transition involving a composition-dependent displacive component, Phys Rev Lett 106(24) (2011) 245701.
[49] J.L. Zhang, C.C. Tasan, M.J. Lai, D. Yan, D. Raabe, Partial recrystallization of gum metal to achieve enhanced strength and ductility, Acta Materialia 135 (2017) 400-410.
[50] M. Fatemi, C.S. Pande, H.R. Child, Detection of several ω-phase morphologies in β-III Ti by small-angle neutron scattering and transmission electron microscopy, Philosophical Magazine A 48(4) (2006) 479-500.
[51] S. Cao, Y. Jiang, R. Yang, Q.-M. Hu, Properties of β/ω phase interfaces in Ti and their implications on mechanical properties and ω morphology, Computational Materials Science 158 (2019) 49-57.
[52] D.L. Moffat, D.C. Larbalestier, The competition between martensite and omega in quenched Ti-Nb alloys, Metallurgical Transactions A 19(7) (1988) 1677-1686.
[53] D. De Fontaine, N.E. Paton, J.C. Williams, The omega phase transformation in titanium alloys as an example of displacement controlled reactions, Acta Metallurgica 19(11) (1971) 1153-1162.
[54] R.G. Hennig, D.R. Trinkle, J. Bouchet, S.G. Srinivasan, R.C. Albers, J.W. Wilkins, Impurities block the alpha to omega martensitic transformation in titanium, Nature materials 4(2) (2005) 129-33.
[55] E. Cerreta, G.T. Gray, A.C. Lawson, T.A. Mason, C.E. Morris, The influence of oxygen content on the α to ω phase transformation and shock hardening of titanium, Journal of Applied Physics 100(1) (2006) 013530.
[56] M. Tane, H. Nishiyama, A. Umeda, N.L. Okamoto, K. Inoue, M. Luckabauer, Y. Nagai, T. Sekino, T. Nakano, T. Ichitsubo, Diffusionless isothermal omega transformation in titanium alloys driven by quenched-in compositional fluctuations, Physical Review Materials 3(4) (2019).
[57] A.E. Pontau, D. Lazarus, Diffusion of titanium and niobium in bcc Ti-Nb alloys, Physical Review B 19(8) (1979) 4027-4037.